electronics

MDPI

Article

Modeling and Design of a New Flexible Graphene-on-Silicon Schottky Junction Solar Cell

Francesco Dell'Olio, Michele Palmitessa and Caterina Ciminelli *

Optoelectronics Laboratory, Politecnico di Bari, via E. Orabona 4, 70125 Bari, Italy; francesco.dellolio@poliba.it (F.D.O.); mipalm@fastwebnet.it (M.P.)
* Correspondence: caterina.ciminelli@poliba.it; Tel.: +39-080-596-3404

Academic Editors: Yoke Khin Yap and Zhixian Zhou
Received: 5 September 2016; Accepted: 19 October 2016; Published: 26 October 2016

Abstract: A new graphene-based flexible solar cell with a power conversion efficiency >10% has been designed. The environmental stability and the low complexity of the fabrication process are the two main advantages of the proposed device with respect to other flexible solar cells. The designed solar cell is a graphene/silicon Schottky junction whose performance has been enhanced by a graphene oxide layer deposited on the graphene sheet. The effect of the graphene oxide is to dope the graphene and to act as anti-reflection coating. A silicon dioxide ultrathin layer interposed between the n-Si and the graphene increases the open-circuit voltage of the cell. The solar cell optimization has been achieved through a mathematical model, which has been validated by using experimental data reported in literature. The new flexible photovoltaic device can be integrated in a wide range of microsystems powered by solar energy.

Keywords: optoelectronic devices; solar cell; Schottky junction; flexible electronics; graphene

1. Introduction

Graphene, which is one of the most promising two-dimensional (2D) materials, is composed of carbon atoms arranged in a hexagonal lattice [1]. It can be synthetized in the form of ultrathin sheets consisting of one or a few atomic layers via several techniques, such as chemical vapor deposition, and it can be easily transferred on different substrates [2].

Graphene has several unique electronic, optoelectronic, mechanical, and thermal properties that make it very attractive in many scientific areas, including nanoelectronics, optoelectronics, and photonics [3].

The research interest on graphene optoelectronics and photonics [4] is quickly growing with the demonstration of high-performing devices such as modulators [5], photodetectors [6], saturable absorbers [7], absorbers in the terahertz regime [8,9], polarization controllers [10], delay lines [11,12], phase shifters [13], and solar cells [14]. In particular, the large mechanical flexibility of graphene, its high conductivity (10^6 S/cm), and transparency (97.7% for graphene monolayer in visible wavelengths) make the use of this material very attractive in the field of photovoltaics [15].

Several enabling operative functions have been envisaged for graphene sheets in photovoltaics technology. Graphene can serve as a transparent conductive electrode in organic or inorganic solar cells [16,17], as an intermediate layer in tandem solar cells [18], and as a barrier layer in perovskite solar cells [19]. Perovskite solar cells in which the electron collection layers are implemented through especially synthetized graphene/TiO_2 nanocomposites have been demonstrated [20], while graphene quantum dots have been used as active layer in a solar cell [21].

By transferring a graphene sheet on a semiconducting substrate of Si or GaAs, a Shottky junction acting as a solar cell under illumination can be manufactured via simple fabrication processes. The first graphene/n-Si Shottky junction solar cell exhibited a quite low efficiency (~1.5%) [22].

By properly optimizing the cell configuration, the efficiency has been improved up to 15.6% [23]. A more expensive graphene/GaAs Shottky junction solar cell with an efficiency of >18% has been reported [24]. These values of efficiency are the best ones for graphene-based solar cells.

One of the key advantages of the graphene/n-Si Shottky junction solar cells is that they can be made flexible by thinning the substrate [25,26]. In this way, flexible solar cells with an efficiency potentially higher than 10% and an excellent environmental stability can be fabricated via a simple and low cost technological process. This feature of the graphene/n-Si Shottky junction solar cells is extremely attractive because flexible solar cells [27] are in demand for a wide range of applications, such as wearable and implantable microsystems and wireless sensor networks for Internet of Things (IoT).

High-efficiency flexible solar cells with good environmental stability, low complexity, and a low manufacturing have not yet been proposed. The state of the art of the efficiency for flexible solar cells is around 30% for GaAs cells manufactured via epitaxial lift-off [28]. However, the only solar cells with an efficiency >10% that can be easily fabricated via a low cost process are the perovskite-based cells [29] (record efficiency = 16.47%), even if at the expense of poor environmental stability [30].

In this paper, we report on the design of a new flexible solar cell based on a Schottky junction consisting of an ultrathin layer of graphene oxide (GO) deposited on a few graphene atomic layers, which are transferred on an n-doped silicon layer (see Figure 1).

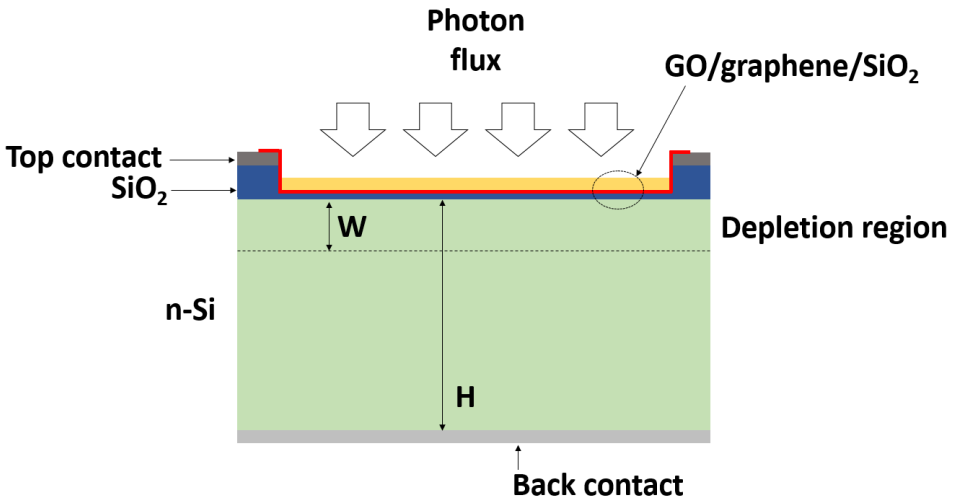

Figure 1. Cross section of the designed Schottky junction solar cell. GO: graphene oxide.

Aiming at maximizing the cell performance, the presence of a silicon oxide layer (thickness <2 nm) between the silicon layer and the graphene sheet has been considered, and the influence of a graphene oxide film (thickness <100 nm) on the top of the graphene sheet has been studied.

The silicon dioxide, with an optimized thickness, increases the open-circuit voltage and consequently the efficiency of the solar cell. The carrier transport across the silicon dioxide ultrathin layer is enabled by the tunnel effect.

The graphene oxide film induces the p-doping of the graphene [31] with a consequent increase of both the work function and the conductivity of the graphene sheet. In addition, the GO film acts as an anti-reflection coating layer, as explained in Section 3.

We assume that the graphene sheet, synthetized by chemical vapor deposition, is transferred on the top of a square Si window patterned in a Si/SiO_2 wafer that is properly thinned to guarantee the desired flexibility. In addition, we assume that, before the graphene transfer, a metal contact (top contact) with a square shape is deposited on the SiO_2 layer around the Si window and another metal contact (back contact) is deposited on the back side of the n-Si. The ultrathin SiO_2 layer can be grown on the n-Si immediately before the graphene transfer by exposing the wafer to clean room air at

room temperature and controlled humidity (average humidity = 42%). In this way, the thickness of the SiO_2 layer slowly increases as the exposure time increases [32]. Alternatively, the ultrathin SiO_2 layer can be grown by immersing the sample in ultrapure water with dissolved oxygen concentration of 9 ppm. For example, by using this technique, a SiO_2 layer with a thickness of 1.5 nm can be grown of an n-doped silicon wafer (donor dopant concentration = 10^{15} cm^{-3}) after an exposure time of 2×10^4 min [32]. After the graphene transfer, a GO solution can be spin-coated on the cell forming a uniform GO layer.

The solar cell design is based on a mathematical model taking into account all physical effects occurring within the Schottky junction when it is illuminated via solar radiation. The model is validated using data from the literature. The device performance has been calculated assuming AM (air mass) 1.5 illumination (power density = 100 mW/cm^2), which is the standard terrestrial spectrum of solar radiation.

2. Solar Cell Model

The complete mathematical model was developed for the design of the solar cell shown in Figure 1. Simpler structures without the GO and the SiO_2 layers can be also studied with the same model.

As is well known, a depletion layer is created in the n-Si in close proximity to the junction. Photons arriving within the silicon layer generate electron-hole pairs both in the depletion layer and outside of it. All of these pairs can contribute to the photo-generated current density J_{ph}.

J_{ph} originates from two contributions—the drift current density J_{dr} and the hole current density J_p. J_{dr} is due to electrons and holes that are generated in the depletion layer by the shorter wavelength light and then accelerated by the built-in electric field towards the metal contacts before they recombine. J_p is due to the holes generated outside the depletion layer by the longer wavelength light. The holes diffuse in the n-Si towards the top contact.

According to [33], the wavelength dependent expressions of J_{dr} and J_p are given by

$$J_{dr}(\lambda) = qF(\lambda)\,T_R(\lambda)\left[1 - e^{-\alpha(\lambda)W}\right], \text{ and} \tag{1}$$

$$J_p(\lambda) = \frac{qF(\lambda)T_R(\lambda)\alpha(\lambda)L_p}{\alpha^2(\lambda)L_p^2-1} e^{-\alpha(\lambda)W}\left[\alpha(\lambda)L_p - \frac{\frac{SL_p}{D_p}\left[\cosh\frac{H'}{L_p} - e^{-\alpha(\lambda)H'}\right] + \sinh\frac{H'}{L_p} + \alpha(\lambda)L_p e^{-\alpha(\lambda)H'}}{\frac{SL_p}{D_p}\sinh\frac{H'}{L_p} + \cosh\frac{H'}{L_p}}\right], \tag{2}$$

where λ is the wavelength, q is the electron charge, F is the photon flux, α is the silicon absorption coefficient, W is the width of the depletion layer, S is the recombination velocity at the back contact, and H' is equal to H-W where H is the thickness of the n-Si layer. L_p is the hole diffusion length given by $(D_p\,\tau_p)^{\frac{1}{2}}$ where D_p is the hole diffusion coefficient and τ_p is the hole lifetime.

$T_R(\lambda)$ is given by $T_{ML}(\lambda)[1\text{-}R(\lambda)]$; $T_{ML}(\lambda)$ is the transmittance of the GO/graphene/SiO_2 multi-layer, and R is the reflectance of the GO-coated graphene/silicon junction. When the cell structure does not include the GO and SiO_2 layers, $T_{ML}(\lambda)$ denotes the transmittance of the graphene sheet, and R the silicon reflectance.

The width W of the depletion layer can be written as [33]

$$W = \left\{\frac{2\varepsilon_s}{qN_D}\left[(\Phi_G - \chi) - \frac{kT\ln(N_C/N_D)}{q} - \frac{kT}{q}\right]\right\}^{1/2}, \tag{3}$$

where ε_s is the silicon dielectric constant, N_D is the donor impurity concentration, Φ_G is the graphene work function, χ is the silicon electron affinity, k is the Boltzmann constant, T is the absolute temperature, and N_C is the effective density of states in the conduction band.

For each value of λ, $J_{ph}(\lambda) = J_{dr}(\lambda) + J_p(\lambda)$. Since silicon absorbs light in the wavelength range from $\lambda_1 = 0.28$ μm to $\lambda_2 = 1.2$ μm, the total photo-generated current is given by the following integral:

$$J_{ph} = \int_{\lambda_1}^{\lambda_2}\left[J_{dr}(\lambda) + J_p(\lambda)\right]. \tag{4}$$

The external quantum efficiency of the cell (EQE), i.e., the number of electron-hole pairs generated for each absorbed photon, is given by

$$\mathrm{EQE}\,(\lambda) = \frac{J_{ph}\,(\lambda)}{qF\,(\lambda)\,T_R\,(\lambda)}. \tag{5}$$

Assuming that the shunt resistance is infinite (see, for example, the experimental data in [22]) and, consequently, its effect on the performance of the cell is negligible, the equivalent electric circuit in Figure 2a models the solar cell.

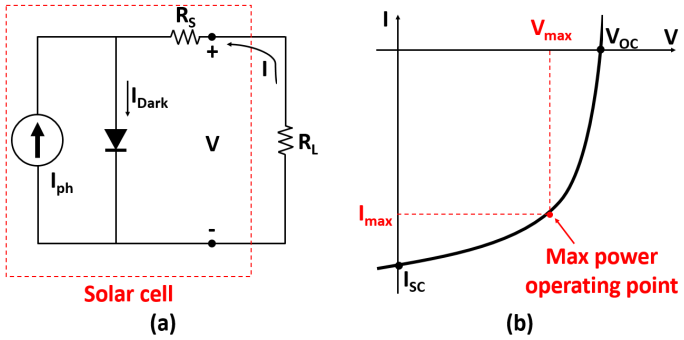

Figure 2. (**a**) Equivalent circuit of the solar cell. (**b**) Qualitative plot of the I–V characteristics of the solar cell.

The current generator represents the photocurrent generation and $I_{ph} = J_{ph}\,A$, where A is the area of the solar cell. The resistance R_S is the series resistance of the solar cell. The diode corresponds to the cell behavior when it is not illuminated by the solar radiation (under this condition $I_{ph} = 0$). The current flowing in the diode is the dark current I_{Dark} equal to

$$I_{\mathrm{Dark}} = I_S\left(\mathrm{e}^{\frac{q(V-IR_S)}{nkT}} - 1\right), \tag{6}$$

where n is the ideality factor, and I_S is the saturation current. I_S can be written as [33,34]

$$I_S = AA^*T^2\mathrm{e}^{\frac{-q(\Phi_G-\chi)}{kT}}\mathrm{e}^{-\delta\sqrt{q\phi_\mathrm{T}}}, \tag{7}$$

where A^* is the effective Richardson constant, ϕ_T (in eV) is the average height of the energy barrier due to the SiO_2 layer, and δ is the thickness of the SiO_2 layer ($\delta = 0$ when there is not a SiO_2 layer interposed between the graphene sheet and the n-Si).

The I–V characteristics (see Figure 2b) of the solar cell is

$$I = I_S\left(\mathrm{e}^{\frac{q(V-IR_S)}{nkT}} - 1\right) - I_{ph}. \tag{8}$$

V_{OC} denotes the open-circuit voltage, which is the voltage across the cell terminals when the load resistance R_L is an open circuit and, consequently, $I = 0$, and I_{SC} denotes the short-circuit current, i.e., the value of I when $R_L = 0$ and, consequently, $V = 0$.

The fill factor FF of the solar cell, which is a measure of the "squareness" of the I–V characteristics, is given by:

$$\mathrm{FF} = \frac{V_{\mathrm{max}}\,J_{\mathrm{max}}}{V_{OC}\,J_{SC}}, \tag{9}$$

where V_{max} and J_{max} are the voltage and the current density at the maximum-power operating point, respectively, i.e., the point of the I–V characteristics of the solar cell where the generated electric power $P = V\,I$ is maximum.

The power conversion efficiency (PCE; sometimes called simply efficiency) is the main performance parameter for any solar cell:

$$\mathrm{PCE} = \frac{V_{\max} J_{\max}}{P_{\mathrm{in}}}, \tag{10}$$

where P_{in} is the incident optical power density.

The model physical parameters used in the simulations are summarized in Table 1. The wavelength-dependent silicon absorption coefficient was derived from experimental data [35] and is shown in Figure 3. The empirical relation reported in [36] was used to take into account the τ_p dependence on N_D. D_p was expressed as kT (μ_p/q), and the analytical expression in [37] was used for the hole mobility μ_p. Data in [31] were used to estimate R_S, the reflectivity $R(\lambda)$, and the wavelength-dependent transmittance of graphene, GO, and SiO_2.

Table 1. Model parameters.

Parameter	Symbol	Value	Reference
Temperature	T	300 K	[34]
Electron affinity of silicon	χ	4.05 eV	[34]
Electron charge	q	1.6×10^{-19} C	[34]
Effective density of states in conduction band	N_C	2.8×10^{19} cm^{-3}	[34]
Ideality factor	n	1.42 (with GO layer)/1.65 (without GO layer)	[31]
Graphene work function	Φ_G	4.92 eV (with GO layer)/4.84 eV (without GO layer)	[31]
Effective Richardson constant	A^*	112 A·cm^{-2}·K^{-2}	[31]
Silicon dielectric constant	ε_s	11.7	[34]
Recombination velocity at the back contact	S	10^{15} cm/s	[38]
Boltzmann constant	k	8.62 eV/K	[34]

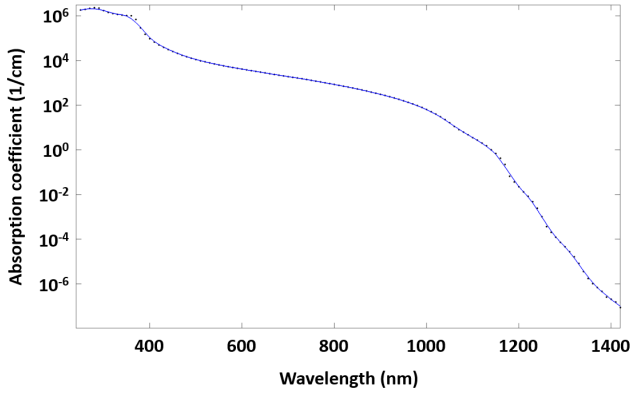

Figure 3. Wavelength-dependent silicon absorption coefficient.

The model was used to calculate the main performance parameters of two graphene-based Schottky junction solar cells reported in the literature. The calculated performance parameters were then compared to the experimental values in the literature, showing a very good model/experiment agreement.

The first device considered for the validation of our model is a solar cell made by a monolayer graphene/ultrathin silicon Schottky junction [25]. The silicon layer is n-doped with $N_D = 2 \times 10^{16}$ cm^{-3} and its thickness is only 10.6 µm. We calculated the J–V curve and the EQE dependence on the wavelength. By comparing the plot obtained by the model with the experimental curves, we noticed a very good agreement, as described below.

Table 2 compares the calculated and measured values of the four key performance parameters, V_{OS}, J_{SC}, FF, and PCE. For the PCE, the difference between calculated and measured values is about 0.3%. For V_{OS}, J_{SC}, and FF the differences are 0.03 V, 1.11 mA/cm^2, and 3.3%, respectively.

Table 2. Calculated vs. measured performance parameters of the solar cell reported in [25].

Measured/Calculated	V_{OC} (V)	J_{SC} (mA/cm^2)	FF (%)	PCE (%)
Measured values [25]	0.416	12.40	25.2	1.30
Calculated values	0.419	13.51	28.5	1.61

The second solar cell simulated by our model is that reported in [31]. It is a cell based on a monolayer graphene/n-Si Schottky junction that has been experimentally studied with and without a GO layer with a thickness of 100 nm on the graphene sheet. The thickness of the silicon layer is 300 µm, and the dopant atoms concentration in this layer is $N_D = 5 \times 10^{15}$ cm^{-3}. Using our model, we simulated the two cells with and without the GO layer. For example, Figure 4a shows the calculated J–V curve for the two cells. Again, the agreement between the calculated (Figure 4a) and the measured curves (Figure 4b) is very good. The same agreement can be observed for the performance parameters (see Table 3) with a difference between calculated and measured values of the PCE less than 0.3%. For V_{OS}, J_{SC}, and FF the differences are <0.015 V, <5 mA/cm^2, and $\leq$5%, respectively.

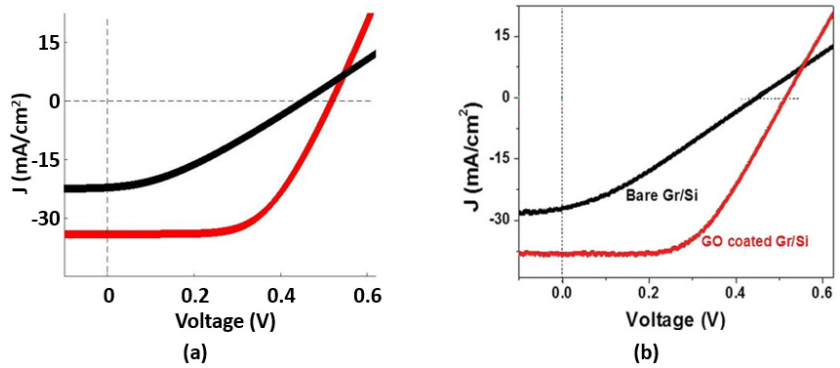

Figure 4. J–V curve for the solar cell in [31]. Black curves refer to the cell w/o graphene oxide (GO). Red curves refer to the cell with GO. (**a**) Calculated data. (**b**) Measured data that are adapted from [31], with the permission of The Royal Society of Chemistry.

Table 3. Calculated vs. measured performance parameters of the solar cell reported in [31].

Measured/Calculated	V_{OC} (V)	J_{SC} (mA/cm^2)	FF (%)	PCE (%)
Measured values (w/o GO) [31]	0.440	27.20	29	3.6
Calculated values (w/o GO)	0.453	22.49	33.14	3.38
Measured values (with GO) [31]	0.512	38.40	53	10.6
Calculated values (with GO)	0.518	34.10	58	10.33

3. Solar Cell Design

Aiming to investigate the influence of silicon doping on solar cell performance, we considered a simple monolayer graphene/n-Si junction with a thickness $H = 10$ µm. This H value assures a very good flexibility of the cell. We varied N_D from 10^{15} to 10^{19} cm^{-3}, and we calculated the relevant values of the PCE (see Figure 5a). As expected, the PCE increases as N_D decreases because both the photo-generated current density J_{ph} and, consequently, the EQE increases when N_D decreases. Due to this PCE dependence on N_D, we chose a light doping of the n-Si layer with $N_D = 10^{15}$ cm^{-3}.

The number of atomic layers forming the graphene sheet has to be optimized because the graphene sheet resistance and, consequently, R_S decrease as the number of atomic layers increases. When R_S decrease, an improvement of the efficiency results, but the graphene optical transmittance and thus J_{ph} are reduced when the number of atomic layers is too high. Considering a graphene/n-Si solar cell with silicon doping $N_D = 10^{15}$ cm^{-3} and $H = 10$ µm, we evaluated the PCE dependence on the number

of atomic layers when this parameter varies from 1 to 5 (see Figure 5b). The best PCE value (=3.02%) was obtained when the number of atomic layers was 3. This result is consistent with experimental results reported in [26].

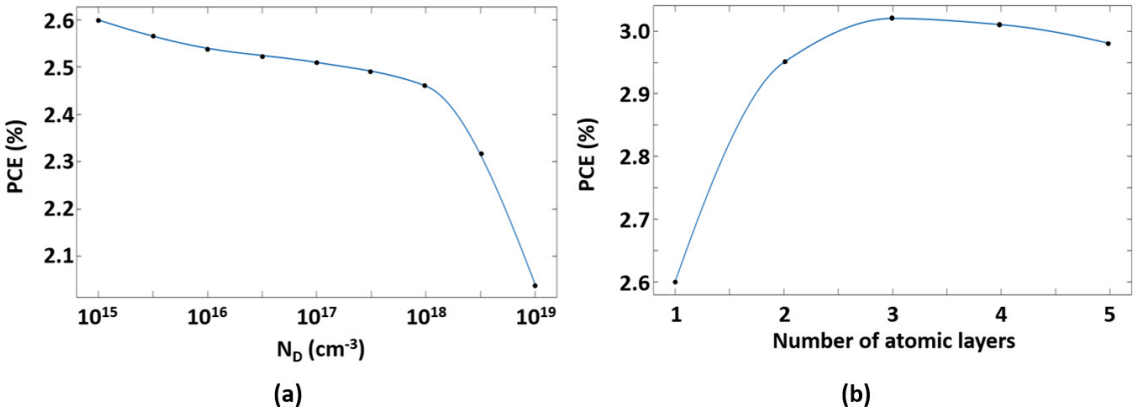

Figure 5. (**a**) Power conversion efficiency (PCE) dependence on N_D for the monolayer graphene/n-Si junction with H = 10 μm. (**b**) PCE dependence on the number of graphene atomic layers forming the graphene sheet, H = 10 μm and $N_D = 10^{15}$ cm^{-3}.

To further increase the PCE of the cell, a quarter-wave anti-reflection coating (ARC) layer can be deposited on the trilayer-graphene. The optimum refractive index of the ARC layer n_{ARC} is the geometric mean of the refractive index of silicon and air [39]. Since the solar energy intensity is maximum at about 0.55 μm [40] and the silicon refractive index at that wavelength is 4.1 [35], the optimum value of n_{ARC} is 2.0, which is very close to the refractive index of a GO layer with a thickness of <100 nm [31]. Thus, a GO layer can be used as ARC. As already mentioned, that layer dopes the graphene sheet, with a further beneficial effect on the cell performance. The optimum thickness of the ARC layer is $\lambda/4n_{ARC}$ = 69 nm at λ = 0.55 μm. Table 4 summarizes the solar cell performance with and without the GO layer and shows that the PCE improves up to 5.31% when the GO is deposited. V_{OS}, J_{SC}, and FF increase due to the deposition of the GO layer of 0.071 V, 5.35 mA/cm^2, and 3.86%, respectively.

Table 4. Performance of the solar cell with and without the GO quarter-wave anti-reflection coating (ARC).

Solar Cell Description	V_{OC} (V)	J_{SC} (mA/cm^2)	FF (%)	PCE (%)
Solar cell w/o GO ARC	0.431	13.27	52.86	3.02
Solar cell with GO ARC (thickness = 69 nm)	0.502	18.62	56.72	5.31

To increase the junction built-in voltage and the open-circuit voltage of the solar cell, one suitable approach is the oxidation of the n-Si surface before the graphene transfer. Figure 6a shows the PCE dependence on the thickness δ of the SiO_2 layer grown by the Si surface oxidation. The PCE monotonically increases as δ increases, but a δ value exceeding 1.5 nm should be avoided because it could prevent the carrier transport through the oxide layer. Therefore, we have chosen δ = 1.5 nm. Figure 6b shows the V_{OC} vs. δ plot. Our simulation confirms that, as δ increases, V_{OC} also increases. In particular, V_{OC} increases from 0.50 to 0.65 V by growing a SiO_2 layer with a thickness in the range from 0 nm to 1.5 nm. In addition, the SiO_2 layer, as expected, does not degrade the photo-generated current density due to its nanometer thickness and, consequently, the cell short-circuit current. The effect of the SiO_2 layer with a thickness of 1.5 nm on the fill factor is an increase in this performance parameter from 56.7% to 64.0%.

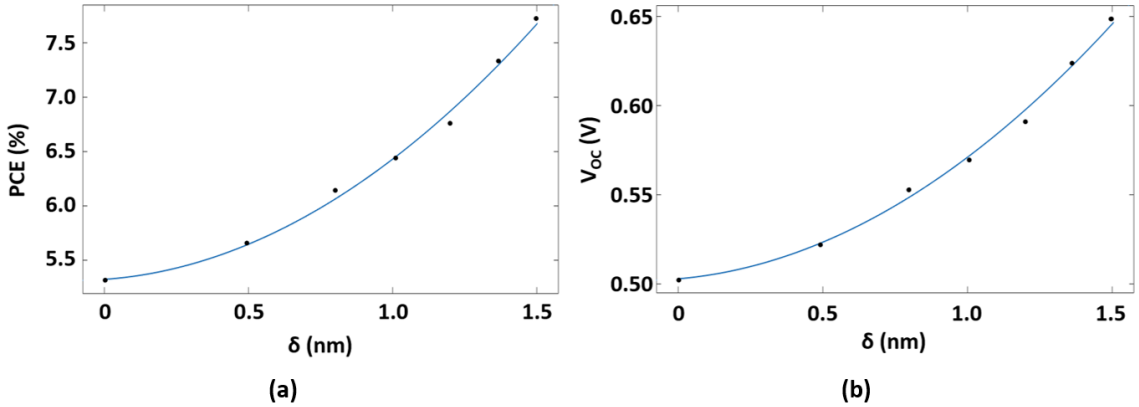

Figure 6. (**a**) PCE dependence on the thickness of the silicon oxide layer. (**b**) Open-circuit voltage vs. δ. Number of atomic layers forming the graphene sheet = 3, solar cell with GO ARC, H = 10 μm, and $N_D = 10^{15}$ cm^{-3}.

Several experimental results [26] have confirmed that silicon/graphene solar cells with a thickness of ≤50 μm are very flexible and do not alter their performance after tens of bending cycles. Thus, we investigated the possibility of increasing the thickness H of the n-Si layer to improve the cell PCE. Figure 7a shows the PCE dependence on H. We can observe that the H increase induces a PCE improvement up to 10.04% for H = 50 μm, mainly due to the increase of the EQE. This physical interpretation is confirmed by the J_{SC} dependence on H (see Figure 7b). The short-circuit current density, which is approximately equal to the photo-generated current density, increases as H also increases. In particular, J_{SC} varies from 18.6 mA/cm^2 to 25.7 mA/cm^2 when H increases from 10 μm to 50 μm.

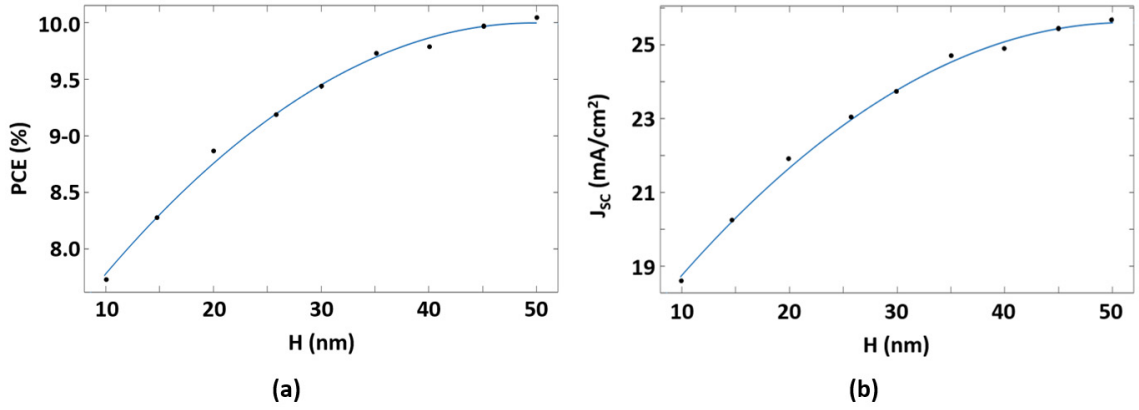

Figure 7. (**a**) PCE dependence on H. (**b**) Short-circuit current density vs. H. Number of atomic layer forming the graphene sheet = 3, solar cell with GO ARC, δ = 1.5 nm, and $N_D = 10^{15}$ cm^{-3}.

The features of the optimized solar cell and its performance are summarized in Table 5.

The envisaged fabrication process of the optimized solar cell includes the patterning of the properly thinned oxidized n-Si substrate by photolithography and wet etching of SiO_2, the deposition of the metal contacts by sputtering, the immersion of the sample in ultrapure water with dissolved oxygen to grow the ultrathin SiO_2 layer, the graphene transfer on that layer, and the deposition of the GO layer by spin coating.

The achieved PCE improves by about 1.6% compared with the state-of-the-art flexible silicon/graphene Schottky junction solar cells, which is 8.42% [26]. To our knowledge, PCE values >10% are achievable in flexible photovoltaic devices on GaAs [41], crystalline silicon (c-Si) [42], copper indium gallium (di)selenide (CIGS) [43], and perovskite solar cells [44]. GaAs, CIGS, and c-Si cells are

very stable, but their fabrication is complex, expensive, or both, while, as already mentioned, the environmental stability of perovskite solar cells is usually lower with respect to competing technologies. The values assumed for the thickness of the graphene sheet and of the SiO_2 layer have been already demonstrated as technologically feasible [23]. The designed flexible solar cell has a fabrication process simpler and cheaper than GaAs, CIGS, and c-Si cells; based on several experimental data [25,26], we expect that it is more stable than perovskite cells. In fact, experiments reported in [25] show that the performance of graphene/silicon Schottky junction flexible solar cells is degraded by only 0.4% after they are exposed to air for 20 days. In addition, cells based on the same technology are quite insensitive to tens (up to 50) of bending cycles (PCE degradation <0.1%) [26].

Table 5. Features and performance of the optimized solar cell.

Parameter	Symbol	Value
Doping of the n-Si layer	N_D	10^{15} cm^{-3}
Number of atomic layer forming the Graphene sheet	-	3
Thickness of the GO ARC	-	69 nm
Thickness of the SiO_2 layer	δ	1.5 nm
Thickness of the n-Si layer	H	50 µm
Short-circuit current density	J_{SC}	25.71 mA/cm^2
Open-circuit voltage	V_{OC}	0.66 V
Fill factor	FF	59%
Power conversion efficiency	PCE	10.04%

4. Conclusions

A new flexible graphene-on-silicon Schottky junction solar cell with a PCE of about 10% has been modeled and designed. This efficiency value improves the state of the art by more than 1.6%. The device has been optimized using a complete mathematical model we have developed. To enhance the solar cell performance, a graphene oxide layer has been used to p-dope the graphene sheet and to reduce the light reflection at the silicon/graphene interface. The open-circuit voltage and consequently the PCE of the solar cell have been increased by an ultrathin silicon oxide layer between the graphene sheet and the n-Si layer, whose thickness has been optimized through a compromise between two opposite needs, i.e., the cell efficiency and its flexibility. The designed cell can be easily manufactured by standard technological processes, and its environmental stability is better with respect to the low-cost competing technologies, such as those based on perovskites. These features of the proposed device enable its potential application in the field of IoT and wearable technology.

Author Contributions: Francesco Dell'Olio supervised the design and wrote the article; Michele Palmitessa performed the mathematical development of the model and designed the device; Caterina Ciminelli conceived the study, supervised the design, and reviewed the paper with particular reference to the physical aspects of the device.

Conflicts of Interest: The authors declare no conflict of interest.

References

1. Warner, J.H.; Schaffel, F.; Rummeli, M.; Bachmatiuk, A. *Graphene: Fundamentals and Emergent Applications*; Elsevier: Waltham, MA, USA, 2013.
2. Choi, W.; Lee, J. *Graphene: Synthesis and Applications*; CRC Press: Boca Raton, FL, USA, 2016.
3. Novoselov, K.S.; Fal'ko, V.I.; Colombo, L.; Gellert, P.R.; Schwab, M.G.; Kim, K. A roadmap for graphene. *Nature* **2012**, *490*, 192–200. [CrossRef] [PubMed]
4. Bonaccorso, F.; Sun, Z.; Hasan, T.; Ferrari, A.C. Graphene photonics and optoelectronics. *Nat. Photonics* **2010**, *4*, 611–622. [CrossRef]
5. Liu, M.; Yin, X.; Ulin-Avila, E.; Geng, B.; Zentgraf, T.; Ju, L. A graphene-based broadband optical modulator. *Nature* **2011**, *474*, 64–67. [CrossRef] [PubMed]

6. Xia, F.; Mueller, T.; Lin, Y.; Valdes-Garcia, A.; Avouris, P. Ultrafast graphene photodetector. *Nat. Nanotechnol.* **2009**, *4*, 839–843. [CrossRef] [PubMed]
7. Bao, Q.; Zhang, H.; Wang, Y.; Ni, Z.; Yan, Y.; Shen, Z.X.; Loh, K.P.; Tang, D.Y. Atomic-Layer Graphene as a Saturable Absorber for Ultrafast Pulsed Lasers. *Adv. Funct. Mater.* **2009**, *19*, 3077–3083. [CrossRef]
8. Yahiaoui, R.; Guillet, J.P.; de Miollis, F.; Mounaix, P. Ultra-flexible multiband terahertz metamaterial absorber for conformal geometry applications. *Opt. Lett.* **2013**, *38*, 4988–4990. [CrossRef] [PubMed]
9. Yahiaoui, R.; Hanai, K.; Takano, K.; Nishida, T.; Miyamaru, F.; Nakajima, M.; Hangyo, M. Trapping waves with terahertz metamaterial absorber based on isotropic Mie resonators. *Opt. Lett.* **2013**, *40*, 3197–3200. [CrossRef] [PubMed]
10. Bao, Q.; Zhang, H.; Wang, B.; Ni, Z.; Lim, C.H.Y.X.; Wang, Y.; Tang, D.Y.; Loh, K.P. Broadband graphene polarizer. *Nat. Photonol.* **2011**, *5*, 411–415. [CrossRef]
11. Conteduca, D.; Dell'Olio, F.; Ciminelli, C.; Armenise, M.N. Resonant Graphene-Based Tunable Optical Delay Line. *IEEE Photonics J.* **2015**, *7*, 7802409. [CrossRef]
12. Tatoli, T.; Conteduca, D.; Dell'Olio, F.; Ciminelli, C.; Armenise, M.N. Graphene-based fine-tunable optical delay line for optical beamforming in phased-array antennas. *Appl. Opt.* **2016**, *55*, 4342–4349. [CrossRef] [PubMed]
13. Capmany, J.; Domenech, D.; Muñoz, P. Silicon graphene waveguide tunable broadband microwave photonics phase shifter. *Opt. Express* **2014**, *22*, 8094–8100. [CrossRef] [PubMed]
14. Yin, Z.; Zhu, J.; He, Q.; Cao, X.; Tan, C.; Chen, H.; Yan, Q.; Zhang, H. Graphene-Based Materials for Solar Cell Applications. *Adv. Energy Mater.* **2014**, *4*, 1300574. [CrossRef]
15. Loh, K.P.; Tong, S.W.; Wu, J. Graphene and Graphene-like Molecules: Prospects in Solar Cells. *J. Am. Chem. Soc.* **2016**, *138*, 1095–1102. [CrossRef] [PubMed]
16. You, P.; Liu, Z.; Tai, Q.; Liu, S.; Yan, F. Efficient Semitransparent Perovskite Solar Cells with Graphene Electrodes. *Adv. Mater.* **2015**, *27*, 3632–3638. [CrossRef] [PubMed]
17. Park, H.; Chang, S.; Zhou, X.; Kong, J.; Palacios, T.; Gradečak, S. Flexible Graphene Electrode-Based Organic Photovoltaics with Record-High Efficiency. *Nano Lett.* **2014**, *14*, 5148–5154. [CrossRef] [PubMed]
18. Tong, S.W.; Wang, Y.; Zheng, Y.; Ng, M.; Loh, K.P. Graphene Intermediate Layer in Tandem Organic Photovoltaic Cells. *Adv. Funct. Mater.* **2011**, *21*, 4430–4435. [CrossRef]
19. Ameen, S.; Shaheer Akhtar, M.; Seo, H.-K.; Nazeeruddin, M.K.; Shin, H.S. An Insight into Atmospheric Plasma Jet Modified ZnO Quantum Dots Thin Film for Flexible Perovskite Solar Cell: Optoelectronic Transient and Charge Trapping Studies. *J. Phys. Chem. C* **2015**, *119*, 10379–10390. [CrossRef]
20. Wang, J.T.; Ball, J.M.; Barea, E.M.; Abate, A.; Alexander-Webber, J.A.; Huang, J.; Saliba, M.; Mora-Sero, I.; Bisquert, J.; Snaith, H.J.; et al. Low-Temperature Processed Electron Collection Layers of Graphene/TiO_2 Nanocomposites in Thin Film Perovskite Solar Cells. *Nano Lett.* **2014**, *14*, 724–730. [CrossRef] [PubMed]
21. Gao, P.; Ding, K.; Wang, Y.; Ruan, K.; Diao, S.; Zhang, Q.; Sun, B.; Jie, J. Crystalline Si/Graphene Quantum Dots Heterojunction Solar Cells. *J. Phys. Chem. C* **2014**, *118*, 5164–5171. [CrossRef]
22. Li, X.; Zhu, H.; Wang, K.; Cao, A.; Wei, J.; Li, C.; Jia, Y.; Li, Z.; Li, X.; Wu, D. Graphene-On-Silicon Schottky Junction Solar Cells. *Adv. Mater.* **2010**, *22*, 2743–2748. [CrossRef] [PubMed]
23. Song, Y.; Li, Y.; Mackin, C.; Zhang, X.; Fang, W.; Palacios, T.; Zhu, H.; Kong, J. Role of Interfacial Oxide in High-Efficiency Graphene—Silicon Schottky Barrier Solar Cells. *Nano Lett.* **2015**, *15*, 2104–2110. [CrossRef] [PubMed]
24. Li, X.; Chen, W.; Zhang, S.; Wu, Z.; Wang, P.; Xu, Z.; Chen, H.; Yin, W.; Zhong, H.; Lin, S. 18.5% efficient graphene/GaAs van der Waals heterostructure solar cell. *Nano Energy* **2015**, *16*, 310–319. [CrossRef]
25. Jiao, T.; Wei, D.; Liu, J.; Sun, W.; Jia, S.; Zhang, W.; Feng, Y.; Shia, H.; Dua, C. Flexible solar cells based on graphene-ultrathin silicon Schottky junction. *RSC Adv.* **2015**, *5*, 73202–73206. [CrossRef]
26. Ruan, K.; Ding, K.; Wang, Y.; Diao, S.; Shao, Z.; Zhang, X.; Jie, J. Flexible graphene/silicon heterojunction solar cells. *J. Mater. Chem. A* **2015**, *3*, 14370–14377. [CrossRef]
27. Pagliaro, M.; Palmisano, G.; Ciriminna, R. *Flexible Solar Cells*; Wiley VCH: Weinheim, Germany, 2008.
28. Lin, Q.; Huang, H.; Jing, Y.; Fu, H.; Chang, P.; Li, D.; Yao, Y.; Fan, Z. Flexible photovoltaic technologies. *J. Mater. Chem. C* **2014**, *2*, 1233–1247. [CrossRef]
29. Yin, X.; Chen, P.; Que, M.; Xing, Y.; Que, W.; Niu, C.; Shao, J. Highly Efficient Flexible Perovskite Solar Cells Using Solution-Derived NiO_x Hole Contacts. *ACS Nano* **2016**, *10*, 3630–3636. [CrossRef] [PubMed]

30. Berhe, T.A.; Su, W.N.; Chen, C.H.; Pan, C.-J.; Cheng, J.-H.; Chen, H.-M.; Tsai, M.-C.; Chen, L.Y.; Dubale, A.A.; Hwang, B.J. Organometal halide perovskite solar cells: Degradation and stability. *Energy Environ. Sci.* **2016**, *9*, 323–356. [CrossRef]
31. Yavuz, S.; Kuru, C.; Choi, D.; Kargar, A.; Jina, S.; Bandaru, P.R. Graphene oxide as a p-dopant and an anti-reflection coating layer, in graphene/silicon solar cells. *Nanoscale* **2016**, *8*, 6473–6478. [CrossRef] [PubMed]
32. Morita, M.; Ohmi, T.; Hasegawa, E.; Kawakami, M.; Ohwada, M. Growth of native oxide on a silicon surface. *J. Appl. Phys.* **1990**, *68*, 1272–1281. [CrossRef]
33. Hovel, H.J. Solar Cells. *Semicond. Semimet.* **1975**, *11*, 112–148.
34. Sze, S.M. *Physics of Semiconductor Devices*; Wiley: New York, NY, USA, 1969.
35. Green, M.A.; Keevers, M.J. Optical properties of intrinsic silicon at 300 K. *Prog. Photovolt. Res. Appl.* **1995**, *3*, 189–192. [CrossRef]
36. Fossum, J.G. Computer-aided numerical analysis of silicon solar cells. *Solid State Electron.* **1976**, *19*, 269–277. [CrossRef]
37. Arora, N.D.; Hauser, J.R.; Roulston, D.J. Electron and hole mobilities in silicon as a function of concentration and temperature. *IEEE Trans. Electron. Devices* **1982**, *2*, 292–295. [CrossRef]
38. Chen, M.J.; Wu, C.Y. A new method for computer-aided optimization of solar cell structures. *Solid State Electron.* **1985**, *28*, 751–761. [CrossRef]
39. Saleh, B.A.E.; Teich, M.C. *Fundamentals of Photonics*; Wiley: Hoboken, NJ, USA, 2007.
40. Goodstal, G. *Electrical Theory for Renewable Energy*; Delmar, Cengage Learning: Clifton Park, NY, USA, 2013.
41. Takamoto, T.; Kaneiwa, M.; Imaizumi, M.; Yamaguchi, M. InGaP/GaAs-based Multijunction Solar Cells. *Prog. Photovolt. Res. Appl.* **2005**, *13*, 495–511. [CrossRef]
42. Cruz-Campa, J.L.; Okandan, M.; Resnick, P.J.; Clews, P.; Pluym, T.; Grubbs, R.K.; Gupta, V.P.; Zubia, D.; Nielson, G.N. Microsystems enabled photovoltaics: 14.9% efficient 14 μm thick crystalline silicon solar cell. *Sol. Energy Mater. Sol. Cells* **2011**, *95*, 551–558. [CrossRef]
43. Chirilă, A.; Buecheler, S.; Pianezzi, F.; Bloesch, P.; Gretener, C.; Uhl, A.R.; Fella, C.; Kranz, L.; Perrenoud, J.; Seyrling, S.; et al. Highly efficient Cu(In,Ga)Se_2 solar cells grown on flexible polymer films. *Nat. Mater.* **2011**, *10*, 857–861. [CrossRef] [PubMed]
44. Halim, H.; Guo, Y. Flexible organic-inorganic hybrid perovskite solar cells. *Sci. China Mater.* **2016**, *59*, 495–506. [CrossRef]